Arabian Journal of Chemistry (2020) 13, 6904–6920

King Saud University

Arabian Journal of Chemistry

www.ksu.edu.sa
www.sciencedirect.com

ORIGINAL ARTICLE

Enhanced cuttings transport efficiency of water-based muds using (3–Aminopropyl) triethoxysilane on polypropylene-nanosilica composite

Jeffrey O. Oseh [a,b,d], M.N.A.M. Norddin [a,b,c,*], Issham Ismail [a,b], Afeez O. Gbadamosi [a,b,d], Augustine Agi [a,b], Abdul R. Ismail [a,b], Prasad Manoger [a,b], Kumaresan Ravichandran [a,b]

[a] *Department of Petroleum Engineering, School of Chemical and Energy Engineering, Universiti Teknologi Malaysia, 81310 Johor Bahru, Malaysia*
[b] *Malaysia Petroleum Resources Corporation Institute for Oil and Gas (MPRC–UTM), Universiti Teknologi Malaysia, 81310 Johor Bahru, Malaysia*
[c] *Advanced Membrane Technology Research Center (AMTEC), Universiti Teknologi Malaysia, 81310 Johor Bahru, Malaysia*
[d] *Department of Chemical and Petroleum Engineering, College of Engineering, Afe Babalola University, Ado–Ekiti P.M.B. 5454, Ekiti State, Nigeria*

Received 19 May 2020; accepted 2 July 2020
Available online 10 July 2020

KEYWORDS

Water-based mud;
Cuttings transport;
Polypropylene;
Nanosilica;
Polymer nanocomposite;
Rheological properties;
(3-Aminopropyl) triethoxysilane;
Cuttings diameters

Abstract The lifting of cuttings has been a challenging phenomenon in the petroleum industry for a long period, given the complexity of different cuttings types and their high tendency to gravitate to the low side of the hole. Although many additives have been applied to improve the efficiency of water-based muds (WBMs) for cuttings transport, only a few success was recorded in the application of these additives once evaluated under different field situations. In this study, a new WBM formulated by nanocomposites was proposed to lift cuttings out of the annulus during drilling. Series of characterization, rheological, filtration loss, and cuttings transport tests were performed on the drilling muds formulated by (3-Aminopropyl) triethoxysilane modified polypropylene-silica nanocomposite (PP-SiO_2 NC-NH_2). The cuttings transport test was conducted in a 16-ft. annulus using 9.5 ppg muds, a 60°-hole angle, and annular velocities between 66.1 and 138.6 ft/min at different PP-SiO_2 NC-NH_2 concentrations of 0.4, 0.5, 0.8, and 1.2 ppb. The performance of 0.5 ppb PP-SiO_2 NC-NH_2 + WBM on CTE was evaluated and compared with that of WBM + 0.5 ppb of partially hydrolyzed polyacrylamide (PHPA) at five different hole angles from 90 to 0°. The results

* Corresponding authors at: Department of Petroleum Engineering, School of Chemical and Energy Engineering, Universiti Teknologi Malaysia, 81310 Johor Bahru, Malaysia.
E-mail addresses: jeffreyonuomaoseh@graduate.utm.my (J.O. Oseh), anam@utm.my (M.N.A.M. Norddin).
Peer review under responsibility of King Saud University.

Production and hosting by Elsevier

https://doi.org/10.1016/j.arabjc.2020.07.004

Nomenclature

10–min	10-minute gel strength
10–s	10-second gel strength
A–0.4	WBM + 0.4 ppb modified NC
A–0.5	WBM + 0.5 ppb modified NC
A–0.8	WBM + 0.8 ppb modified NC
A–1.2	WBM + 1.2 ppb modified NC
API	American petroleum institute
APTES	(3–aminopropyl) triethoxysilane
AV	Apparent viscosity
B–0.5	WBM + 0.5 ppb PHPA
BM	base mud
CTE	cuttings transport efficiency
CTEs	cuttings transport efficiencies
D_{50}	particle median diameter
EtOH	ethanol
FCT	filter cake thickness
FL	filtrate loss volume
GS	gel strength
HPHT	high-pressure high-temperature
LD	laser diffraction
NaOH	sodium hydroxides
NC	nanocomposite
NCs	nanocomposites
$–NH_2$	amino groups
NH_4OH	ammonium hydroxide
NP	nanoparticle
NPs	nanoparticles
–OH	hydroxyl groups
PAC HV	high viscosity polyanionic cellulose
PE–b–PEG	polyethylene–block poly (ethylene glycol)
PNC	polymer nanocomposites
PNCs	polymer nanocomposites
PP	polypropylene
PP-SiO_2 NC	polypropylene–silica nanocomposite
PP-SiO_2 NC-NH_2	modified polypropylene-nanosilica composite by APTES
PSD	particle size distribution
PV	plastic viscosity
ROP	penetration rate
SiO_2 NP	nanosilica/silica nanoparticle
SMD	Sauter mean diameter of particles based on surface area
SSA	specific surface area by laser diffraction
TEM	transmission electron microscopy
TEOS	tetraethyl orthosilicate
WBM	water-based mud
YP	yield point
ζ–potential	zeta potential

of zeta potential showed that the PP-SiO_2 NC-NH_2 was stable. The rheological and filtration properties were enhanced by the inclusion of PP-SiO_2 NC-NH_2 in the WBM. There exists a better enhancement in the CTE of PP-SiO_2 NC-NH_2 + WBM over that of PHPA + WBM at 0.5 ppb. The highest cuttings lifted to the surface occurred in a vertical well, followed by 90°, 30°, 60°, and 45° wells. An increase in annular velocity and the orbital motion of the drill pipe by mechanical action increased the CTE of the nanocomposite more than the rest mud samples. It seems the PP-SiO_2 NC-NH_2 can be more effective than the PHPA for the drilling process and can improve the cuttings lifting performance of WBMs but caution should be exercised to ensure its proper dispersion in drilling muds.

1. Introduction

The implementation of rotary drilling has made the circulation of drilling fluids to take place inside and out of the drill pipe to clean the rock cuttings that are created from the fragmented rock (Ismail et al., 2016; Caenn et al., 2017). The cuttings exhibited two different characteristics, they jammed the bit teeth, and those on the bottom hole are lifted through the annulus to the surface separating facility. The latter of these characteristics is termed cuttings transport. The arrival of horizontal and extended-reach wells shown that the decrease in transported rock cuttings has become noticeable and the cleaning of the wellbore is exacerbated as well depths and hole deviation rise (Gbadamosi et al., 2018a,b). The faster slipping velocities compel cuttings to gravitate and accrue on the bottom of the hole (Lyons et al., 2016). With this event, the density of the mud is more liable to rise to the extent that can lead to the fractured formation and circulation loss (Fattah and Lashin, 2016). If the rock cuttings accrual carries on, the tendency of the cuttings to form beds at the low sidewall of the hole will increase. This phenomenon can result in severe drilling problems, such as increased torque and drag, an impediment to pipe movement into and out of the hole, and often pipe sticking occurs, this increases downtime and drilling cost extensively (Boyou et al., 2019; Oseh et al., 2019a,b). To combat these problems of poor cuttings transport, many rheological modifiers have been designed. These modifiers are xanthan gum, guar gum, low and high viscosity polyanionic cellulose (PAC-Lv and PAC-Hv), carboxyl methylcellulose (CMC), bentonite, dispersant viscosity modifiers (DVM), partially hydrolyzed polyacrylamide (PHPA), etc. (Hale and Mody, 1993; Luz et al., 2017). However, these modifiers are either expensive, harmful, toxic, or cannot perform satisfactorily under different downhole conditions where temperature,

pressure, and other variables vary disproportionately. As for the PHPA, the most highly sought polymer for field applications owing to its ability to extend bentonite clay in low-solids mud (Hale and Mody, 1993; Lam et al., 2015), its major flaws are loss of its shear-thinning character under the static ageing condition and the possibility of excessive gel strength and viscosity of its mud thereby hindering the cuttings transport performance.

The recent birth of polymer nanocomposites (PNCs) is seen as one of the most state-of-the-art technologies of this era by several studies, especially in the oil and gas industry given their efficacy to enhance the properties of conventional WBMs resulting from their fine dispersibility and less-viscous character (Youssef et al., 2017; Xu et al., 2018). These studies reported improvement in the rheology, lubricity, filtration control, and clay swelling inhibition of WBMs with the PNCs. These products also appeared to minimize pipe sticking (Mao et al., 2015; Youssef et al., 2017), minimalized torque and drag during hole tripping, and increases the hole stability (Jain et al., 2016; Xu et al., 2018). This is mainly because of their synergistic effects from applying the advantages of a polymeric and nanoscale agent. The composited nanosilica or silica nanoparticle (SiO_2 NP) with polymers, such as polypropylene (PP) has been another hotspot of interest in different fields of research (Bitinis et al., 2011; Zu et al., 2013). This is because such hybrid of synthetic PP and inorganic SiO_2 NP (termed PP-SiO_2 NC) can result in an ordered physical entanglement and/or stable chemical crosslinking between the PP and SiO_2 NP, especially if the colloidal nanosilica is efficiently dispersed with the PP matrix (Thangaraj et al., 2019). PP is efficient in improving the clearing of cuttings from the drilled hole due to its viscoelastic property and the aptitude to exert a buoyancy force on rock cuttings (Katende et al., 2019). SiO_2 NP has been used largely as a PNC-based mud in most laboratory works to decrease water loss, inhibit clay swelling, and enhance viscosity mainly for its efficient temperature resistance, excellent strong bond connection, surface functionality, large surface-area-to-volume ratio, small size, and easy to disperse when modified (Elochukwu et al., 2017).

Several investigations on SiO_2 NP composites with polymers have shown that to efficiently exploit the full potentials of this colloidal particle with a polymer blend, there is the need to improve its dispersion with such polymer by using silane coupling agents, namely (3-Aminopropyl) triethoxysilane (APTES) (Omurlu et al., 2016; Cao et al., 2017). The APTES cations have been identified to improve the dispersion and stability of nanosilica suspension when the cations are adsorbed onto the nanosilica surface to neutralize the concentrations of silanol groups (Si-OH) and stabilize the colloids for stable particle formation (Qiao et al., 2015). Hence, APTES attachment onto the surface of the developed PP-SiO_2 NC was considered in this study to prevent any possible agglomeration of the nanocomposite (NC) and make it more stable in the drilling mud system. Therefore, in this study, a developed PP-SiO_2 NC modified by APTES (termed PP-SiO_2 NC-NH_2) was used to enhance the properties of conventional WBM under different types of sand grains, such as granite, sandstone, limestone, and dolomite. The rheological characteristics, filtration properties, and the cuttings transport performance of the PP-SiO_2 NC-NH_2 were exclusively examined and compared with the WBM and 0.5 ppb PHPA mud sample.

2. Experimental

2.1. Materials

The chemicals used to synthesize and modify the PP-SiO_2 NC-NH_2 are as follows: PP having a melt index of 12.3 g per 10 min with a Chemical Abstracts Service (CAS) number of 9003-07-0, ammonium hydroxide (NH_4OH), xylene, 98% reagent grade tetraethyl orthosilicate (TEOS) with a CAS number of 78-10-4, polyethylene-b-poly (ethylene glycol) (PE-b-PEG) of weight ratio 50:50 (PE: PEG) with a CAS number of 97953-22-5, APTES of 97% reagent grade with a CAS number of 13822-56-5, and ethanol (EtOH). The chemicals used to formulate the drilling muds include bentonite, caustic soda (NaOH), soda ash (Na_2CO_3), xanthan gum (XG), high viscosity polyanionic cellulose (PAC HV), barite, and PHPA with a CAS number of 17194–82–0. These chemicals were acquired from Sigma-Aldrich (M) Sdn. Bhd., Selangor Malaysia and were applied as purchased.

2.2. Methods

2.2.1. Synthesis and formation mechanism of the nanocomposite

The synthesis and formation of the NC particles were carried out based on a previous report (Zu et al., 2013) with some changes. The synthesis involves two phases, which are hydrophobic and hydrophilic. For the hydrophobic phase, synthetic PP of 6 g was mixed with the co-polymer PE-b-PEG of 24 g at 300 °F and a torque-speed of 300 rpm in a Plasti-Corder Brabender. Xylene of 20 ml was used to dissolve the mixture and the dissolved mixture was stirred at 280 °F and 300 rpm for 2 h with a magnetic agitator. TEOS of 20 ml was slowly added into the sample and the stirring was continued until a pure solution was achieved. The sample was added gently into the hydrophilic solution prepared by mixing 60 ml of NH_4OH and 100 ml of EtOH. The stirring of the sample continued for an extra 30 min at 170 °F. The sample was cooled for 24 h at ambient temperature. It was separated by the method of centrifugation for 40 min at 6000 rpm. The product obtained was washed with EtOH to eliminate any contaminants and oven-dried for 24 h at 140 °F. The dried product was denoted as PP–SiO_2 NC. Fig. 1 illustrates the synthesis and formation of the particles of PP–SiO_2 NC.

2.2.2. Zeta potential investigation of acquired TEOS

Before the synthesis, the ζ–potential magnitude of the SiO_2 precursor, TEOS was measured by dispersing 0.001 ml of the TEOS in 100 ml of deionized water, as stated in previous research (Wang et al., 2006) to comprehend the level of negativity of the surface charge of the TEOS. Malvern Zetasizer Nano ZSP (Malvern Instruments Inc. Westborough MA, USA) was used to determine the ζ–potential magnitude of the acquired TEOS, and the result indicated that the TEOS has a ζ–potential number of −0.4 mV, as shown in Fig. 2. This value indicates incipient instability that can lead to fast particle agglomeration. The negative surface charge of the synthesized NC is due to the presence of hydroxyl groups (–OH) present on the surface of the formed NC attributed to the SiO_2 NP (Elochukwu et al., 2017).

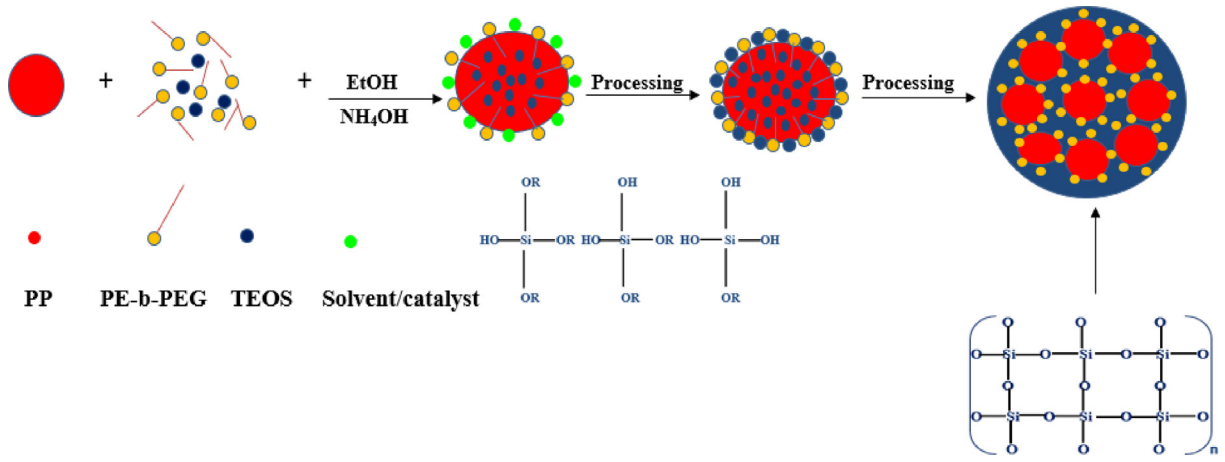

Fig. 1 Synthesis and formation of the nanocomposite.

2.2.3. Relationship between the zeta potential of the developed nanocomposite and bentonite

After the synthesis, the ζ–potential magnitudes of the developed PP-SiO_2 NC and sodium bentonite particles at different levels of pH at ambient temperature (25 °C) were measured using Malvern Zetasizer Nano ZSP (Malvern Instruments Inc. Westborough MA, USA). 0.001 g of the NC was dispersed in 100 ml of deionized water containing 0.1 M HCl and 0.1 M NaOH and the pH was varied between 1.0 and 10.0. The same procedure was implemented to measure the ζ–potential magnitude of the sodium bentonite and the results are presented in Fig. 3, which showed the variation of ζ–potential of the sodium bentonite and synthesized NC with varied pH before modifications by amines. The result verifies that at any pH level, the surface of the synthesized NC and bentonite particles are negatively charged. The magnitudes of these charges found in these two products decreased with increasing pH of the aqueous medium. The developed NC possesses a strongly negative surface charge at all conditions of the pH. When the level of the pH reached 8.0, the ζ–potential of the PP-SiO_2 NC displayed a maximum negative surface charge of −7.22 mV indicating that at this state sufficient –OH is present on the surface of the developed NC. Similarly, the aqueous bentonite system, a pH-dependent product also showed a negative surface charge which is liable for the electrostatic repulsion effect often experienced between bentonite and SiO_2 NP mud system (Barry et al., 2015; Elochukwu et al., 2017). The consequence of these two products having negative surface charges when applied in WBMs is the deflocculation of the mud which could be detrimental to the yield point and gel strength thereby reducing the mud's capacity to transport and suspend drilled cuttings. Given this reason, surface charge modification was carried out on the developed NC using APTES.

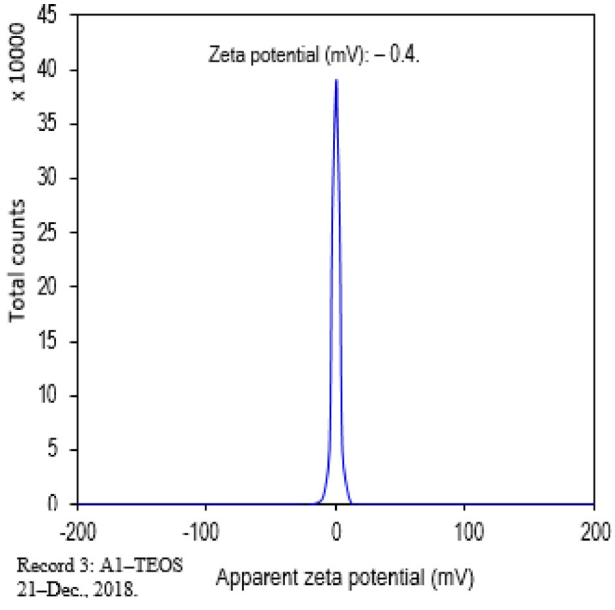

Fig. 2 Surface charge of acquired TEOS.

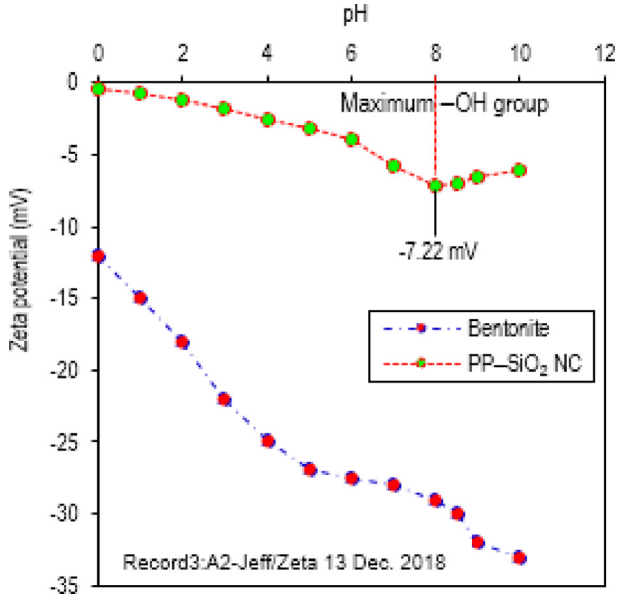

Fig. 3 ζ-potential versus pH for bentonite and synthesized nanocomposite.

2.2.4. Surface modification and zeta potential of PP–SiO_2 NC

Coupling agents, such as organosilanes are used to provide a bond and enhance the adherence between filler and matrix (Qiao et al., 2015). The type of the functional group on the surface of SiO_2 NP can typically determine the surface characteristics of SiO_2 NP-based composites. APTES molecules are the most common organosilanes used in SiO_2-based composite due to their efficiency in increasing the nanosilica dispersion and stability when the molecules are grafted onto the nanosilica surface to reduce the concentrations of Si-OH groups and make the colloids stable (Qiao et al., 2015). The method used to alter the surface charge of the synthesized NC follows the report of a previous investigation (Jafarzadeh et al., 2012).

Four different concentrations (0.4, 0.5, 0.8, and 1.2 ppb) of the synthesized NC were modified. These concentrations were introduced into a prepared solution of 40 ml EtOH/100 ml deionized water. The mixture was homogenized for 10 min at 25 °C with Silverson Homogenizer. A constant amount of 1.4 ml of APTES was gently introduced into the solution and stirred for 10 min. After the stirring, ultrasonication energy was used to further disperse the mixture at 60 °C for 10 min to enhance their dispersion efficiency, while the pH was fine-tuned to a constant level of 8.0 using 0.50 M NaOH. This process condition was maintained for all the concentrations of the synthesized NC to understand the effect of the pH on the varied NC concentrations. Thereafter, the mixture was placed in a centrifugation machine at a torque-speed of 6000 rpm for 40 min, and the supernatant was decanted. The precipitates were washed with EtOH to eliminate any contaminants, freeze-dried, and labeled as modified PP-SiO_2 NC or PP-SiO_2 NC–NH_2. By grafting the cationic APTES dispersant on the NC, an ionic attraction occurs leading to having a positive charge amino group (–NH_2) grafted to the synthesized NC surface through the negative –OH group, as presented in Fig. 4. The modification of the NC in terms of particle stability and size distribution was further confirmed by using the measurement of ζ-potential and laser diffraction techniques, respectively.

2.2.5. Characterization of PP-SiO_2 NC and PP-SiO_2 NC-NH_2

For the ζ-potential investigated at 25 and 150 °C, 0.001 g of each concentration (0.4, 0.5, 0.8, and 1.2 ppb) of the modified and unmodified NCs dried powder samples were dispersed in 100 ml of deionized water and measured by Malvern Zetasizer Nano ZSP (Malvern Instruments Inc. Westborough MA, USA). The pH of the dispersion was adjusted to 8.0 by using 0.1 mol/l solutions of NaOH. The samples were introduced into the pure zeta cells, and the results for each sample were registered as an average of three measurements. Thereafter, the particle size distribution (PSD) and the specific surface area of the NCs were measured by laser diffraction (LD) particle size analyzer (Ultra-high speed Malvern Mastersizer-3000, Westborough MA, USA). The LD instrument generates volume-based particle size distributions and permits the PSD of the test sample to be measured directly. 1.0 g of dried powder samples of the NCs were dispersed in 100 ml deionized water. 1.0 ml of the dispersed particles (wet samples) were fed into the measuring cell and a laser light beam passed through the cell, the wet samples scattered the light making a scattered pattern that was obtained at 52 detectors. The angles and the total diffracted or scattered light patterns were calculated using the Mie scattering model to produce the PSD of spheres that would provide the corresponding scattering pattern. The surface area was calculated indirectly from the diameter distribution of the spherical particles using Eq. (1) according to ISO 13320-1 (2009) testing protocols and the LD assumes that all the measured particles are solid and spherical. That is, it is founded on an ideal state not always found in some materials. The application of this technique permits different important parameters to be obtained from single testing and characterizes a sample more efficiently in a shorter time.

$$SSA = \frac{6\sum \frac{V_i}{D_i}}{\rho_m \sum \frac{D_i}{V_i}} = \frac{6}{\rho_m \times SMD} \tag{1}$$

Using Eq. (1), *SSA* is the calculated specific surface area of the test sample (m^2/g) determined indirectly by the LD from the Sauter mean diameter. *Vi* represents the relative volume by the class size of the particle D_i (cm^3), ρ_m defines the density of the material (g/cm^3), and *SMD* is the Sauter mean diameter based on surface area (nm), which is referred to as the diameter of a sphere having the same surface as the test sample. The Transmission Electron Microscope (TEM) (Hitachi JEM-2100UH, Japan) operating at 200 Kev was used to determine the morphology of the NCs.

2.2.6. Formulation of drilling muds

Table 1 shows the acronyms of the different mud samples formulated. All the mud samples were formulated to have a mud

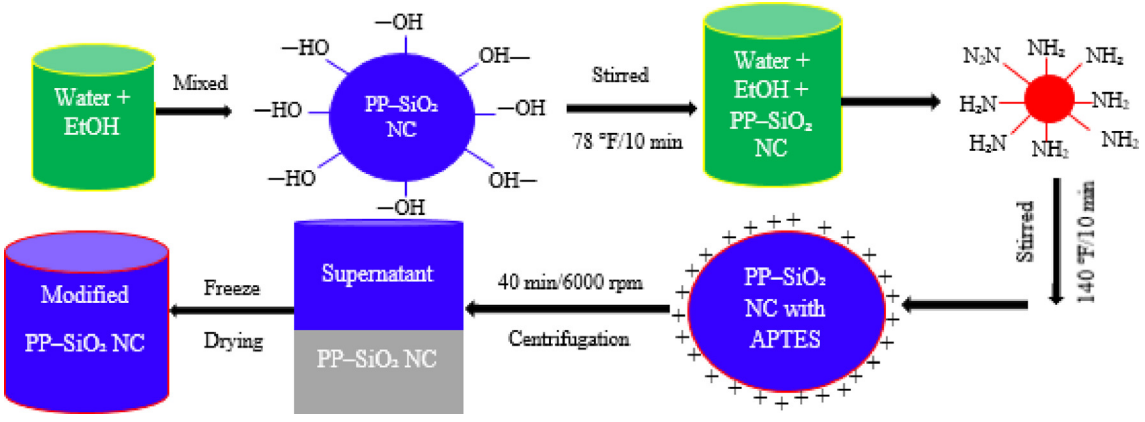

Fig. 4 Surface charge functionalization of developed PP-SiO_2 NC.

weight of 9.5 ppg, based on the recommendation contained in a previous study (Fattah and Lashin, 2016), where mud weight from 9.0 to 10.0 ppg was suggested as the optimal mud formulation for WBMs. The formulation of the mud samples was carried out following the API testing protocols (API RP 13B-1., 2017). The mud samples were formulated to have a high YP and YP/PV ratio to ensure better lifting capacity in the cuttings transport process. The concentrations (0.4, 0.5, 0.8, and 1.2 ppb) of the modified NC were sonicated for 2 h at ambient temperature before their inclusion into the WBM after barite mixing. A standard of 1.0 ppb of additive, which is equivalent to 1 laboratory barrel (350 ml) of drilling fluid was used, as shown in Table 2.

2.2.7. Rheological measurements

The mathematical model, Bingham plastic basic equations, which remains prevalent for description in the field (Wiśniowski et al., 2020) was used to evaluate the rheological properties of WBMs following the drilling mud test protocol (API RP 13B-1., 2017). The Bingham plastic is a linear rheological model that provides the calculation of the apparent viscosity (AV), plastic viscosity (PV), and yield stress (YP) of drilling mud systems. The viscometer dial reading (θ) at the rotational speeds (600 rpm and 300 rpm) was measured by 6-speed Fann viscometer before and after ageing of mud samples at 78 °F (25 °C) and 300 °F (150 °C), respectively. The drilling muds were poured into the heater cup of Fann viscometer until they reached the marked point and the rotor was perfectly immersed in the inscribed line. The motor was switched on and the sleeve was turned to 600 rpm. The dial reading for 600 rpm ($\theta 600$)was registered after the dial attained a stabilized value. To determine the 300 rpm, the sleeve was turned to 300 rpm and the reading was again registered for the 300 rpm ($\theta 300$)after the rotor has stabilized. The AV (mPa-s), PV (mPa-s), and YP (mPa) for each sample was determined by calculating Eqs. (2)–(4), respectively. Gel strength (GS) of 10 s (10-s) was measured by shearing the mud at high speed and then making it rest for 10-s. The maximum value of shear stress reading at 3 rpm after the resting time was found as a 10-s gel. To measure the 10 min (10-min) GS, the same process was followed except; the sample was made to rest for 10-min. The GS readings were registered in mPa. The same process was followed to determine all the rheological properties after keeping the samples inside an ageing cell of the 4-roller oven for 16 h at 300 °F.

Table 1 Different mud samples and acronyms in this research.

Mud sample	Acronyms
WBM	BM
WBM + 0.4 ppb modified NC	A–0.4
WBM + 0.5 ppb modified NC	A–0.5
WBM + 0.8 ppb modified NC	A–0.8
WBM + 1.2 ppb modified NC	A–1.2
WBM + 0.5 ppb PHPA	B–0.5

Table 2 Different compositions of mud samples prepared in this research.

Mud samples	Mud compositions in a laboratory scale for 9.5 ppg weighted mud
BM	320.34 ml water + 15 ppb bentonite + 0.25 g NaOH + 0.25 g Na_2CO_3 + 0.20 g XG + 2.0 g PAC HV + 34.22 g barite.
A–0.4	320.21 ml water + 15 g bentonite + 0.25 g NaOH + 0.25 g Na_2CO_3 + 0.20 g XG + 2.0 g PAC HV + 33.95 g barite + 0.4 ppb modified NC.
A–0.5	320.13 ml water + 15 g bentonite + 0.25 g NaOH + 0.25 g Na_2CO_3 + 0.20 g XG + 2.0 g PAC HV + 33.93 g barite + 0.5 ppb modified NC.
A–0.8	320.11 ml water + 15 g bentonite + 0.25 g NaOH + 0.25 g Na_2CO_3 + 0.20 g XG + 2.0 g PAC HV + 33.65 g barite + 0.8 ppb modified NC.
A–1.2	320.01 ml water + 15 g bentonite + 0.25 g NaOH + 0.25 g Na_2CO_3 + 0.20 g XG + 2.0 g PAC HV + 33.35 g barite + 1.2 ppb modified NC.
B–0.5	320.13 ml water + 15 g bentonite + 0.25 g NaOH + 0.25 g Na_2CO_3 + 0.20 g XG + 2.0 g PAC HV + 33.93 g barite + 0.5 ppb PHPA.

$$AV = \theta 600/2 \tag{2}$$

$$PV = \theta 600 - \theta 300 \tag{3}$$

$$YP = 0.511(\theta 300 - PV) \tag{4}$$

2.2.8. Filtration measurements

API filtrate loss (API FL) measurements were performed with a Fann API filter press. A 100 psi (0.69 MPa) pressure was injected through a nitrogen cylinder from the top and the muds were forced to go through a filter paper placed at the bottom of the cylinder. The measurement was made for 30 min at ambient temperature. The mud that seeps through the filter paper was collected in a test tube and the volume was measured in ml, representing the API FL. The thickness of the filter paper was measured with a Vernier caliper representing the API filter cake thickness (API FCT). The same process was repeated to measure the high-pressure high-temperature (HPHT) filtrate loss volume (HPHT FL) and HPHT FCT after keeping the samples in an ageing cell inside a 4-roller oven for 16 h at 300 °F. The test differential pressure and the temperature in the heating jacket was 500 psi (3.45 MPa) and 300 °F, respectively. For accurate test data, the tests were performed thrice and average readings were registered.

2.2.9. Preparation of drilled cuttings

Table 3 gives an overview of the specification of some of the physical properties of the different types of sand grains used to evaluate the CTEs of the mud samples in this study. The grains were sieved into four different diameters, ranging from 0.50 to 0.85 mm, 1.00 to 1.70 mm, 2.00 to 2.40 mm, and 2.80 to 3.20 mm. The sieved grains were washed and dried thoroughly before injecting them into the flow loop.

Table 3 Specifications of some of the physical properties of types of sand grains.

Sand grains properties	Types of sand grains			
	Sandstone	Granite	Limestone	Dolomite
Specific gravity	2.20–2.80	2.60–2.80	2.60–2.75	2.75–2.90
Average density (ppg)	20.45	23.28	21.78	24.12
Moh's hardness	6.0–7.0	7.0	3.0–4.0	3.5–4.0
Color	Dark grey	Pink	Tan	Grey
Water absorption (%)	< 1.0	0.25	< 1.0	< 0.1
Porosity (%)	0	0.5–1.5	< 1.0	< 0.1
Texture	Medium grained	Coarse grained	Coarse crystalline	Coarse crystalline

2.3. Evaluation of sand cuttings in a flow loop using different drilling mud samples

A field-scale down cuttings transport flow loop was built purposely to investigate the efficiency of drilling muds in the cuttings transport process at ambient temperature, as presented in Fig. 5. The flow loop has been designed to simulate closely field conditions in vertical and low hole angles (0–30°), deviated (31–89°), and horizontal (90°) wellbores according to a previous study (Boyou et al., 2019). The annular test section simulates a cased hole of 60.96 mm (2.4–in.) inner diameter and a rotatable drill pipe with an outer diameter of 30.48 mm (1.2–in.). The rotatable drill pipe was placed inside the acrylic pipe to create a concentric (0% eccentricity) annulus. A representation of the flow loop is shown in Fig. 6.

The formulated mud samples can be driven at flow rates that reflect the range of annular velocities experienced in the field. A liquid flow gauge was installed in the flow loop to estimate the annular velocity throughout the tests and for precise

Fig. 6 Schematic of cuttings rig simulator.

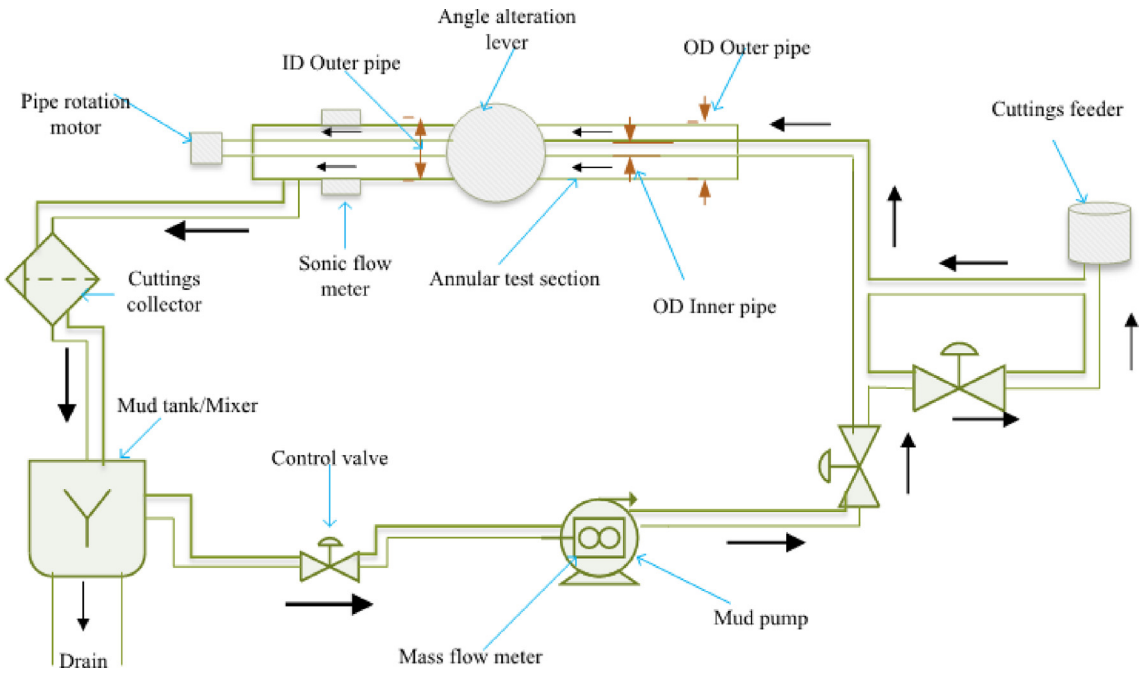

Fig. 5 Schematic of cuttings rig simulator with various apparatus.

data, the sensor was located at the midpoint of the annular test section. The test flow rates were in the range between 20 L/min (0.02 m^3/min) and 42 L/min (0.042 m^3/min). The experiments were conducted using four different annular mud velocities starting from 66.1 ft/min (20.1 m/min), 92.4 ft/min (28.2 m/min), 118.8 ft/min (36.1 m^3/min), and to a maximum value of 138.6 ft/min (42.2 m/min). The annular test section was set at a constant pipe angle of 60° for the investigation of BM and BM + PP-SiO_2 NC-NH_2 at three different concentrations (0.4, 0.8, and 1.2 ppb) of the modified NC without a rotatable inner drill pipe. Thereafter, the pipe angle was varied from 0°, 30°, 45°, 60°, and 90° from the vertical to mirror a complete wellbore and in this case, only the concentration of 0.5 ppb with sandstone cuttings was used for comparison between the modified NC and PHPA in the WBM.

0.5 ppb concentration was selected because drag-reducing polymer, such as PHPA could be more effective when its concentrations are lower as to higher concentrations (Hale and Mody, 1993). Besides, it may be difficult to pump and circulate the muds effectively with the available pump capacity of 42 L/min (0.042 m^3/min) if the PHPA concentration is greater than 0.5 ppb. This is because long-chain PHPA molecules with anionic character at high concentrations can induce high equivalent circulation density (Hale and Mody, 1993). The CTEs were determined both when the pipe was set to rotate at 150 rpm and when it was static. 200 g of each of the test sand was added into the cuttings rig simulator through the cuttings feeder for each test. The drilling muds were circulated using a 2–HP variable speed centrifugal pump with the capacity of 150 L mud tank connected to the pump. The cuttings were separated from the muds by using a cuttings separator of 0.2 mm wire mesh. The lifted cuttings were recovered after seven minutes of the circulation process and five minutes of recirculation to clean out any remaining cuttings inside the circulation pipes before conducting a new experiment. The tests were performed three times and the averages recorded. The cuttings transport efficiency (CTE) was calculated by measuring the rate at which the cuttings were removed from the rig simulator to the rate at which the cuttings were initially injected into the rig simulator.

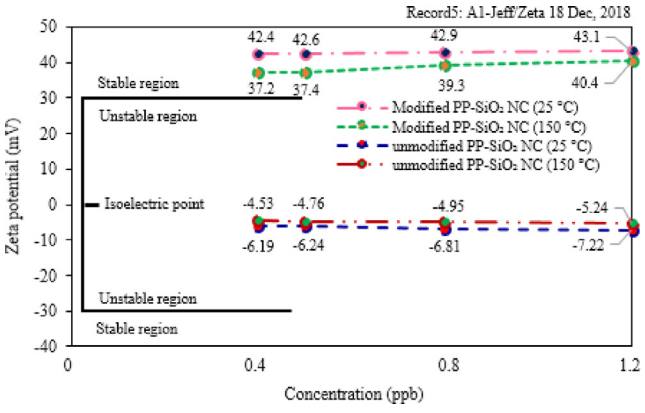

Fig. 7 . ζ–potential of modified and unmodified PP–SiO_2 NC samples.

3. Results and discussions

3.1. PP-SiO_2 NC surface charge and stability

The ζ-potential results of the modified and unmodified NC samples were determined at 25 °C (78 °F) and 150 °C (300 °F). These results are shown in Fig. 7. As can be seen in this figure, all the tested samples of the unmodified product showed negative ζ–potential numbers before and after ageing tests. The negativity of this charge increased at a higher temperature of 150 °C. According to stability indicator of colloids, all these tested samples are unstable, which could be detrimental to mud's properties, such as the YP and GS of drilling mud containing bentonite particles. This is due to the effect of electrostatic repulsion between the unmodified samples and bentonite particles that could lead to aggregation and deflocculation of the particles (Elochukwu et al., 2017). Elucidating further, there exists a slight variation in the ζ-potential data of the unmodified NC at 25 °C shown in Fig. 7 to that of the unmodified NC data reported earlier in Fig. 3 due to the difference in their processing conditions. As mentioned previously, the ζ–potential data shown in Fig. 3 were obtained at different levels of pH that ranged from 1.0 to 10.0, while those presented in Fig. 7 were measured at a constant pH of 8.0. This difference in processing variables is responsible for the slight variation in the ζ–potential data reported in these two figures of the unmodified samples. However, - with 1.2 ppb concentration at 25 °C (Fig. 7), the ζ–potential of the unmodified NC which occurred at −7.22 mV corresponds to that of the unmodified NC (Fig. 3) obtained at a pH of 8.0 where the –OH groups are maximum. It then implies that the –OH groups on the surface of the synthesized NC could have been sufficiently reduced by the positive –NH_2 groups. After modification, the modified samples shifted to a high net positive magnitudes as can be observed in Fig. 7 because of the efficiency of APTES to endow a positive surface charge on the NC. These particles showed strong stability at a high temperature of 150 °C, which indicates their long term lasting effect in high-temperature environments. It can be concluded that the developed NC is physically stable when it was modified by APTES under alkaline environment (pH of 8.0) and they have unfavourable negative surface charges without modification, exemplifying that the modification targets are met. Hence, cuttings transport experiments were conducted using the modified NC (PP-SiO_2 NC-NH_2).

3.2. PSD observation

The PSD results of the NCs with and without surface modification in dilute aqueous solution are shown in Fig. 8. It can be observed that the shapes of the curves in Fig. 8a and b are similar, but the PP-SiO_2 NC-NH_2 sample (Fig. 8b) showed a wider particle distribution than those of the unmodified samples due to the presence of APTES molecules in the modified product (Fig. 8b). It was also observed that the particle sizes of both NCs were more concentrated below 400 nm, in which the unmodified sample ranged from 77 to 370 nm with the median diameter (D_{50}) of 184 nm and mean diameter of 122 nm (Fig. 8a), while that of the modified is distributed between 80

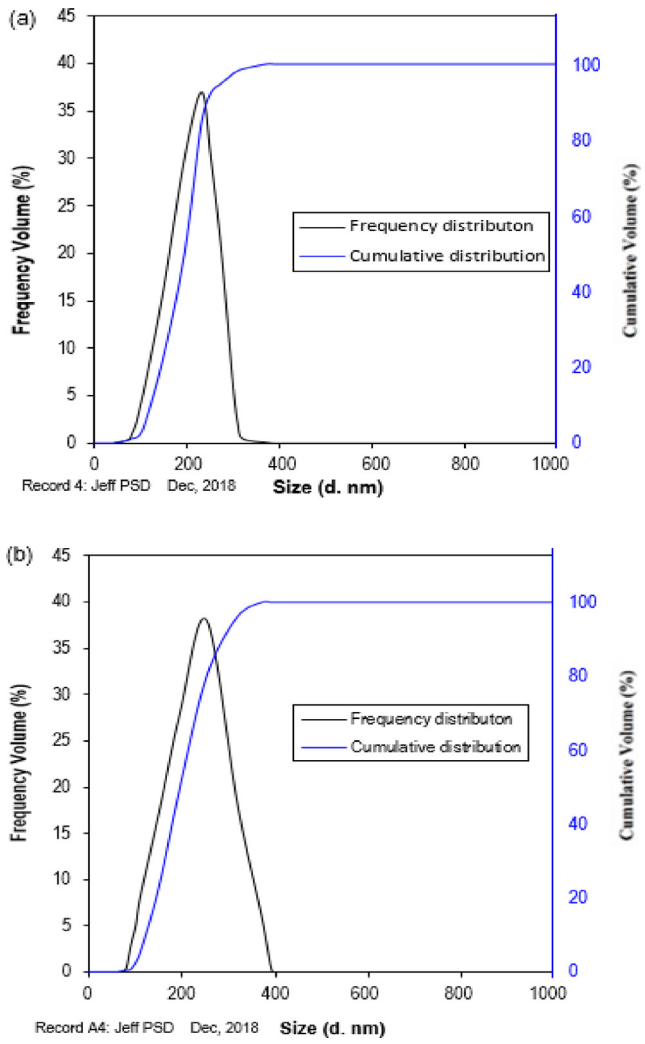

Fig. 8 PSD results of (a) Unmodified NC and (b) modified NC.

and 390 nm with a D_{50} of 189 nm and mean diameter of 146 nm (Fig. 8b). This result indicates that both NC particles have narrow size distributions range within the nanometer domain.

3.3. Laser diffraction specific surface area

Table 4 presents the results of the specific surface area of the modified and unmodified NC samples obtained indirectly from the diameter distribution of particle size by LD technique. It can be observed that these specific surface areas (18.6 m^2/g for unmodified) and (13.7 m^2/g for modified) are reasonably enough for effective interaction with other additives of the WBMs.

Table 4 Specific surface area of modified and unmodified PP–SiO_2 NC by laser diffraction.

Sample	Median particle diameter (D_{50})	Sauter mean particle diameter (SMD)	Laser diffraction SSA
PP–SiO_2 NC	184 nm	122 nm	18.6 m^2/g
PP–SiO_2 NC–NH_2	189 nm	146 nm	13.7 m^2/g

3.4. TEM images of modified and unmodified PP–SiO_2 NC

Fig. 9 depicts the TEM micrographs of the NCs in a dilute aqueous solution. It confirms that the unmodified NC (left) was partially found in low aggregate form and showed irregular shape, while the modified particles (right) appears to show regular circular/spherical shape with a smooth surface indicating that they are well-dispersed. The average particle size observed with TEM was 186 nm for unmodified NC and 192 nm for modified NC, which were consistent with the D_{50} numbers of 184 nm (unmodified NC) and 189 nm (modified NC) of the PSD data, further verifying that the product synthesis and modification met the design goal.

3.5. Rheological properties observation

A precise comprehension of the rheological characteristics is needed to guarantee that cuttings transport and wellbore cleaning are appropriately in place in a drilling situation. The data and discussions of these properties are presented in Figs. 10–15. The AV of the drilling muds is shown in Fig. 10. The modified NC concentrations and 0.5 ppb PHPA before and after hot rolling tests significantly modified the rheology of the BM and increases the AV. However, the highest AV data were observed in the PHPA samples and they are considerably larger than the AV values of the BM and 1.2 ppb of modified NC by 61.5% and 47% before aging and by 60% and 35% after ageing tests, respectively. The fast formation of PHPA long-chain during shearing and the stability of its macro-molecular structure increased its viscosity (Gbadamosi et al., 2019). The AV of the BM with 1.2 ppb of the modified NC was the largest of all the mud samples of the NC though it is only 0.5 mPa.s higher than that of 0.8 ppb. The increase in the AV of the NC mud samples could have resulted from the size of the NC and relatively large surface-area-to-volume ratio which increases the friction between the absorbed water molecules and the particles. In terms of WBM viscosity, water molecules could directly interact with the polymeric chains through hydrogen bonds with its hydrophilic groups to increase their intermolecular forces, hence, the rheological properties (Medhi et al., 2020). With the increase in temperature, fluids often showed a decrease in rheological properties, especially the viscosity and YP. It can also be observed that the AV data of the modified NC and PHPA muds are significantly higher than that of the BM after the ageing test but the drop in the AV of the NC mud systems is smaller compared to that of PHPA due to less degradation of the mud's component of the NC.

Fig. 11 shows the PV values of the drilling muds before and after thermal ageing tests. The shape of the trend lines of the PV is similar to that of the AV. The based mud showed a decrease in PV both before and after ageing tests. For modified NC, an increase in PV over the BM was observed in all the concentrations at the two temperatures considered. For 0.4 and 0.5 ppb, an increase in the PV was observed at a constant value of 27.3%. Also, it was increased by 45.5% for 0.8 and

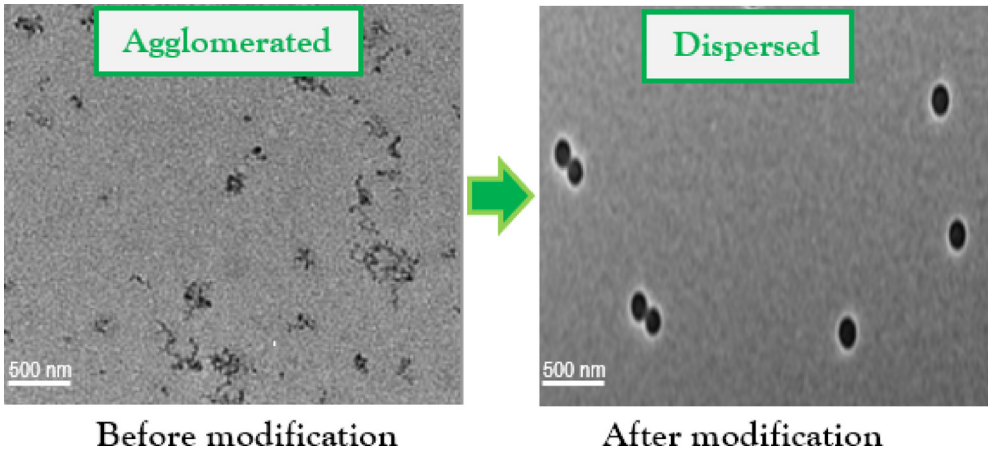

Fig. 9 TEM micrographs of unmodified (left) and modified (right) diluted PP-SiO_2 NC.

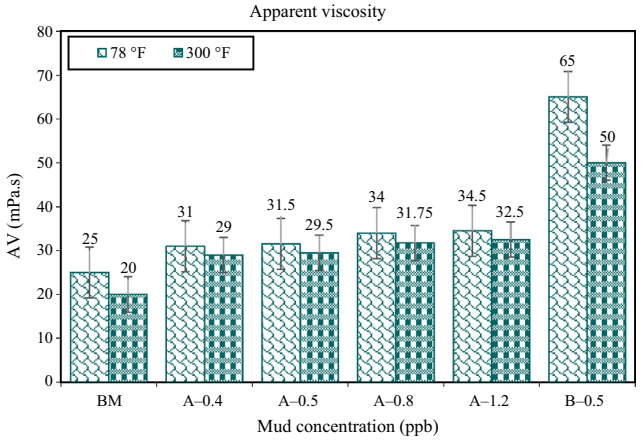

Fig. 10 Apparent viscosity data of modified and unmodified PP-SiO_2 NC.

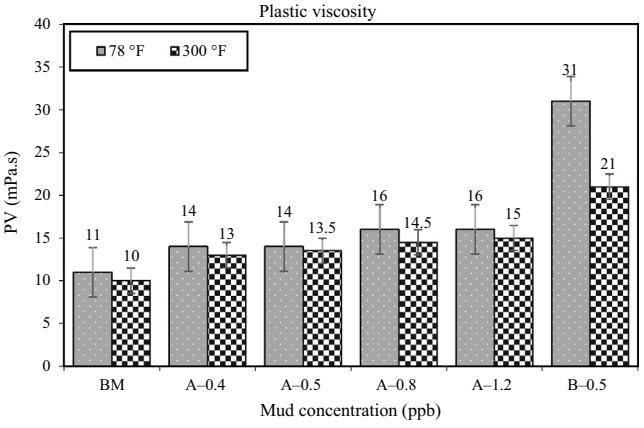

Fig. 11 Plastic viscosity data of modified and unmodified PP-SiO_2 NC.

1.2 ppb. The hydrogen atoms present in the modified NC formed hydrogen bonds with water molecules, and the strength of their intermolecular interactions increased, which improved the rheological properties of the NC mud systems (Medhi et al., 2020). The NC just like the based mud showed a decrease in PV at elevated temperature but the margin of the decrease was very minimal. It increased the PV of the base mud by 30, 35, 45, and 50% with 0.4, 0.5, 0.8, and 1.2 ppb, respectively. The range of the PV values of the modified samples illustrated a flat viscosity profile and they are thermally stable, which could be a desirable feature for drillings in shallow, deep-water formations, and geothermally heated wells. By the inclusion of 0.5 ppb PHPA, the AV data of the BM significantly increased by 181.9% but decreased by 110% after heat treatment, which should be a concern for its performance at bottom-hole conditions. The viscosity enhancement of the PHPA sample is linked to its molecules. The molecules of PHPA are a flexible chain that remains in a coil-like structure in the lack of a shearing effect. These molecules in a coil-like structure led to higher entanglement, low ionic strength, and high charge repulsion of PHPA flexible chains, which is the principal element in the viscosity of PHPA. For the reduction in PHPA sample after ageing, the amide groups of the long-chain go through intense hydrolysis into a carboxylic acid and these hydrolyzed products get precipitated when faced with higher temperatures. This factor makes the long-chains of the PHPA get cut-off, and as a result, the decrease in viscosity (Song et al., 2006).

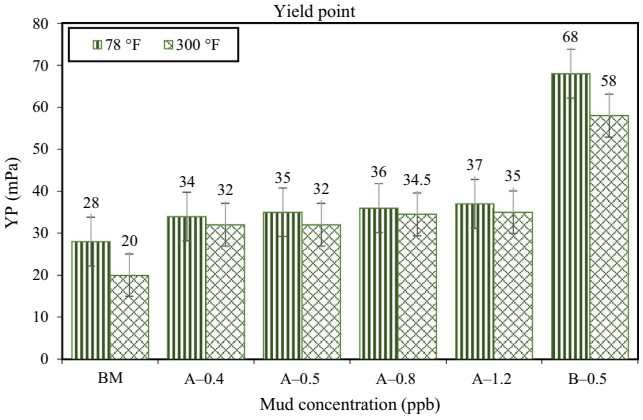

Fig. 12 Yield point data of modified and unmodified PP-SiO_2 NC.

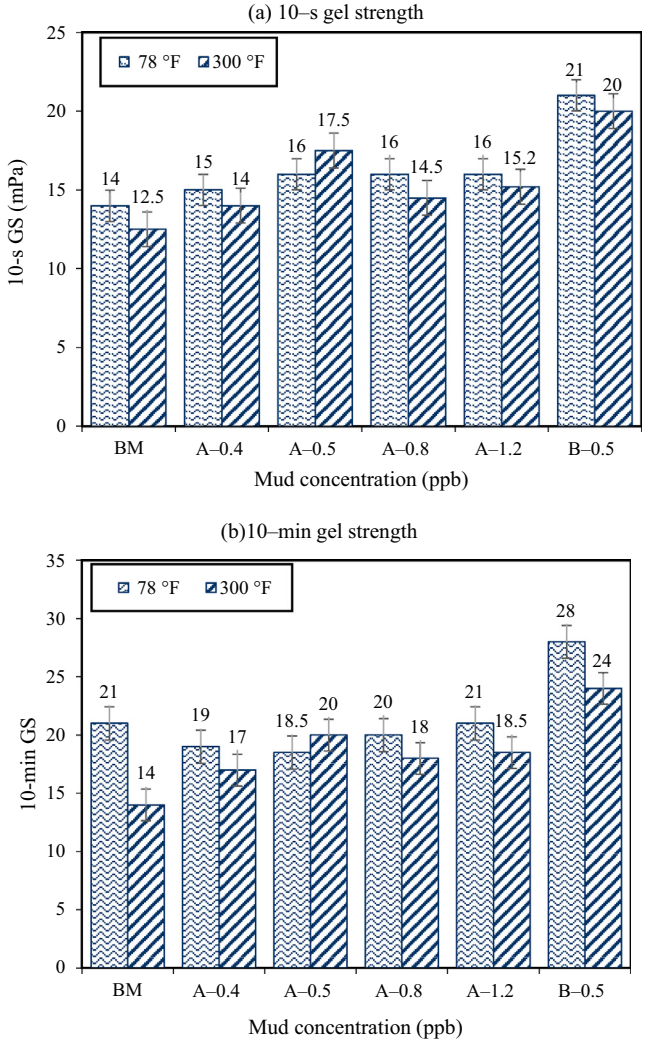

Fig. 13 (a) 10-s and (b) 10-min gels data of modified and unmodified PP-SiO_2 NC.

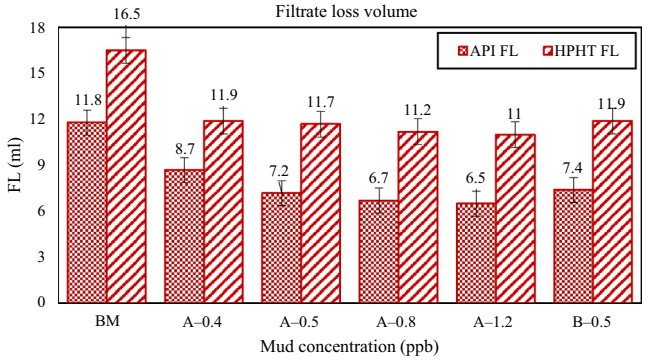

Fig. 14 Filtrate loss control data of modified and unmodified PP-SiO_2 NC.

Fig. 12 depicts the YP values of the drilling muds. Substantial variation exists in the YP values of the modified NC and 0.5 ppb PHPA before and after thermal ageing tests. It can be seen that the YP of the BM was increased with an increase in the concentration of the modified NC. The inclusion of 0.4, 0.5, 0.8, and 1.2 ppb NC concentrations increased the YP of the BM by 21.4, 25, 28.6, and 32.1%, respectively, while the inclusion of 0.5 ppb PHPA displayed a significant increase in the YP by 142.9% before ageing and 190% after ageing tests. The modified NC consist of a relatively large surface area (13.7 m^2/g) and it will increase the interaction of the NC with the matrix and surrounding WBM. This surface area may serve as sites for bonding with functional groups to influence chain entanglement and, thus, can generate a variety of properties in the matrix, such as improved AV, PV, YP, and GS (Medhi et al., 2020). Commenting on the NC samples after the ageing test, in which muds often exhibit a decrease in AV, PV, and YP, the 0.4 ppb displayed a decrease in the YP by a minimal 5.4% when exposed to 300 °F. For 0.5 ppb, the reduction was also minimal by 5.9%. Also, with an increase in the NC concentration to 0.8 ppb, the margin of reduction was found to be further scaled-down by 4.2% and rises to 5.4% for 1.2 ppb, while the 0.5 ppb PHPA sample showed a higher decrease in the YP by 14.7%. However, the highest reduction in the YP after thermal ageing test occurred in the mud sample of the based mud by 28.6%. The reductions in the YP after ageing interprets the temperature sensitivity of the mud samples, especially the base mud sample. High temperatures can break down the components of drilling muds and changes their performance Thus, with the increase in the level of YP of the BM before and after ageing, modified NC demonstrated the noteworthy amount of thermal stability with an increase in their concentration. A further observation in Fig. 12 seems to imply that the NC and PHPA samples can enhance the capacity of the BM to lift more cuttings but the PHPA sample needs high shear stress to be circulated in the annular environment, which could lead to more pump power requirement thereby increasing the cost of drilling. Given the range of the YP which ought to be between 10 and 45 mPa, as recommended by API protocols (API, 2017), all the samples of the NC could be a - suitable choice for cuttings transport.

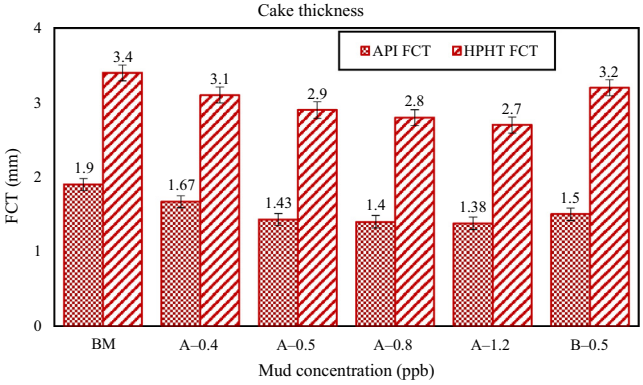

Fig. 15 Cake thickness data of modified and unmodified PP-SiO_2 NC.

Fig. 13 describes the gel behavior of the mud samples before and after thermal ageing tests. The 10-s gels of the BM increased with all the modified NC concentrations and with the 0.5 ppb PHPA at 78 °F and 300 °F (Fig. 13a). However, for the 10-min gels at 78 °F, the behaviour reversed for all the NC concentrations except 1.2 ppb where no change for 10-min gels was observed, while an increase in the 10-min gel by 33.3% was found only for 0.5 ppb PHPA sample (Fig. 13b). It

can be established that the improved 10-s gels of the NC mud systems before ageing - is due to the electrostatic force between the NC which causes the NC to link together with the WBM within 10-s and 10-min period to form a rigid structure. This phenomenon will increase the gelling effect. The reduction observed is a very small margin which could be due to less intermolecular attraction of the particles with the WBM after a prolonged static condition (Oseh et al., 2019c). The less agglomeration or the ineptitude of the NC to agglomerate very fast once the circulation halts could have also reduced the 10-min gels of the NC samples. Moreover, this translates that less pump pressure will be needed to push the mud after resting for 10-min. 0.5 ppb PHPA sample exhibited the highest GS over all the other mud systems at both temperature conditions, indicating that intermolecular forces of attraction (gelling feature) is strongest in the long-chain molecules of PHPA. Nonetheless, the concern with the PHPA sample was that after prolonged hot rolling at a high temperature of 300 °F for 16 h, it displayed less temperature resistance by 14.3% for 10-min gels while the most degraded concentration of the NC (1.2 ppb) reduced by 11.9%. Despite observing a reduction in the 10-min gels, the NC concentrations also showed strong temperature resistance that contributed to preserving the gels at bottom hole environments. This character will guarantee proper drilled cuttings and barite suspension, thus, avoiding sagging issues.

3.6. Filtration properties observation

Other mud properties investigated are the filtrate loss (API and HPHT FL) and cake thickness (API and HPHT FCT). These properties are shown in Figs. 14 and 15, respectively. A good drilling mud must ensure that filtrate loss to the formation is not excessive to cause formation fracture or formation instability. An observation of Fig. 14 appeared to verify that the modified NC has a significant impact on the filtration control property of the BM with an increase in concentration and can remarkably enhance it. From 0.4 to 1.2 ppb concentration of the NC, the API FL control of the BM was improved by 26.3%, 39%, 43.2%, and 45%, respectively. The API FL of the BM was best controlled with 1.2 ppb NC concentration that showed a reduction in the API FL by 45%. This event occurred because the interaction between the dispersed modified NC and water molecules formed an interlocking net over the pores or fractures and prevent other particles in the fluid from passing through (Medhi et al., 2020; Oseh et al., 2020a,b). For 0.5 ppb PHPA concentration, the API FL of the BM was reduced by 37.3%. The filtrate loss control of drilling mud systems can be enhanced using PHPA which aid to block the pore throats of drilling formations and provide encapsulation. Also, PHPA molecules have been proven to link effectively with bentonite particles in the control of water loss. The bentonite particles–PHPA molecules can form a relatively thin filter cake to provide a better sealing, a factor often cited as an advantage for applying PHPA in a bentonite drilling mud system (Hale and Mody, 1993). At the bottom-hole environments, the HPHT FL control of the BM has the highest margin of improvement by 33.3% with 1.2 ppb concentration of the NC. The rest of the NC concentrations improved the HPHT FL of the BM with increasing concentration, by 27.9% for 0.4 ppb, 29% for 0.5 ppb, and 32% for 0.8 ppb, while 0.5 ppb PHPA showed about 29% enhancement in the filtrate loss control of the BM at bottom-hole environments. These data confirmed that PP-SiO_2 NC-NH_2 when added into WBM showed a noticeably reducing trend of filtrate loss of the mud with increasing concentration of the NC product.

A higher filtrate loss volume implies a thicker filter cake. The API and HPHT FCT values of the different mud systems are presented in Fig. 15. For the prepared WBM, its cake thickness under API and bottom-hole conditions were reduced moderately by the micro-NPs and 0.5 ppb PHPA. Before thermal ageing, the decreased in the FCT of the BM occurred in the following way with an increase in the NC concentration: 12.1%, 24.7%, 26.3%, and 27.4% by 0.4, 0.5, 0.8, and 1.2 ppb, respectively, whereas the 0.5 ppb PHPA decreased the cake thickness by 21.1% (API FCT) and 5.9% (HPHT FCT). After exposure to downhole conditions, the NC decreased the cake thickness by 8.8% for 0.4 ppb, 14.7% for 0.5 ppb, and 17.6% for 0.8 ppb. The best fit (1.2 ppb NC concentration) in decreasing the fluid loss appeared to reduce the HPHT FL of the BM by 20.1%. Thus, all the concentrations of the studied NC under the prevailing conditions are worthy of filtrate loss control and can prevent formation fracture and loss of drilling fluids during drilling operations. Expounding further on the rheological and filtration data obtained in this research, it can be inferred that the studied PP-SiO_2 NC-NH_2 particles exhibited remarkable characteristics and showed a significant - degree of temperature stability with an increase in their concentration. If these characteristics persist for even higher values of temperature, it holds a lot of promise in the bottom-hole environments.

4. Cuttings transport observation

4.1. Influence of modified PP–SiO_2 NC on cuttings transport efficiency without pipe rotation

Efficient cuttings removal by circulating drilling mud plays key roles in drilling operations because if the cuttings are not cleared effectively from the drilled hole, they will hinder the drilling. The CTEs for sandstone, granite, limestone, and dolomite cuttings at a constant cuttings diameter that ranged between 0.50 and 0.85 mm (smallest cuttings) were compared using different annular velocities at a constant hole inclination of 60° to comprehend the influence of the modified NC on the cuttings carrying capacity of the prepared WBM system. These data are presented in Fig. 16. As can be observed, the trend of this plot showed that the CTE of the BM was increased by the inclusion of modified NC. At all annular velocities considered, the impact of the NC in the WBM was least for 0.4 ppb and 0.8 ppb, in which the 0.8 ppb was some margins greater than the CTEs of 0.4 ppb, and the greatest impact was observed with 1.2 ppb. The increase in CTE of the NC mud system with an increase in concentration resulted from the effects of electrostatic attraction. The electrostatic attraction will proceed in WBM between modified NC and bentonite particles through face-to-face interaction (i.e. between negative-face bentonite particles and positive-face modified NC particles) and edge-to-face interaction (i.e. between positive-edge bentonite particles and negative-face bentonite particles). This interaction caused the rheological properties to improve as the concentration of the NC increases due to greater attractive

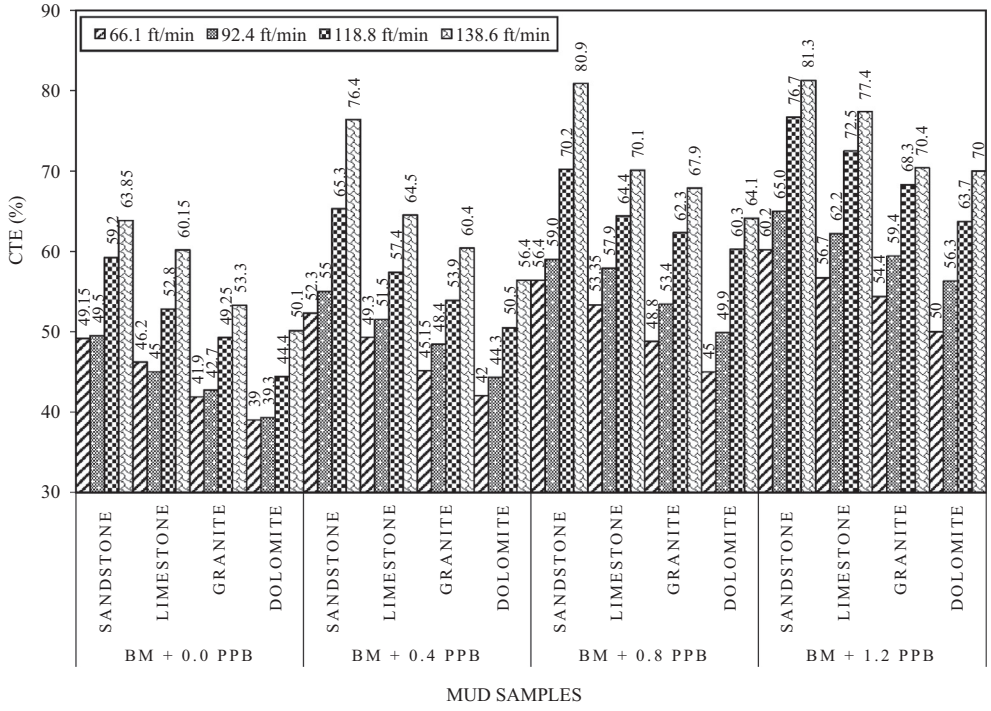

Fig. 16 Different drilling mud systems on CTE for cuttings sizes of 0.50–0.85 mm and constant hole angle of 60° without pipe rotation.

force occurrence, hence, increased colloidal interaction between the mud system and cuttings. This phenomenon contributed to the improvements in the cuttings transport performance of the NC mud systems.

It can also be found in Fig. 16 that the CTE of all the different kinds of cuttings increased with increasing annular velocity from 66.1 to 138.6 ft/min. For these different cuttings types circulated with 1.2 ppb mud system, the sandstone cuttings were lifted greatest to the surface, followed by limestone, next was granite, and the least was dolomite. The margin of increase in CTE exhibited by sandstone over limestone, granite, and dolomite was 5.81%, 9.63%, and 16.9%, respectively, when the lowest annular velocity of 66.1 ft/min was used. When the flow velocity was increased to 138.6 ft/min (largest velocity), sandstone was still the most recovered cuttings at the surface. Limestone showed the fewest margin of decrease behind sandstone by 4.8% while the largest margin was recorded by dolomites by 13.9%. The granite was 13.4% fewer of its recovered cuttings behind sandstone. The same trend of data can also be seen with 92.4 ft/min and 118.8 ft/min. Overall, sandstone grains were the most transported to the surface at all flow velocity and concentration of NC, which could be due to their lowest specific gravity, as reported in Table 3, which makes them experience the lowest gravity effect that was effectively overcome by drag and lift forces (Katende et al., 2019). It can then be concluded that the transport of sandstone cuttings is the easiest of all the sand grains, the NC mud properties of PV = 16 mPa.s (Fig. 11) and YP = 37 mPa (Fig. 12) for A-1.2, and the largest annular velocity of 138.6 ft/min are the most optimum parameters for cuttings transport as per the prevailing conditions.

4.2. Influence of 150 rpm pipe rotation speed on CTE

Tests were conducted using the BM, 0.5 ppb modified NC, and 0.5 ppb PHPA at 0° (vertical), 30°, 45°, 60° (deviated), and 90° (horizontal) with a fixed flow rate of 42 L/min (0.042 m^3/min) on different sandstone grains sizes. The results from these tests are shown in Figs. 17–20 with and without pipe rotation speed of 150 rpm. It can be observed that the profiles of all the plots (bar charts) of various sizes of sandstone grains without pipe rotation are similar to those with pipe rotation at all hole angles examined with decreasing trend of CTE as the cuttings size increases. The CTE of the BM exhibited the lowest percent in the cuttings transport process. The inclusion of 0.5 ppb each of NC and PHPA increased the mud's carrying capacity at all hole angles and cuttings sizes. The NC concentration in the BM proved to circulate the highest percentage of cuttings out of the annular environment. The CTE (A-0.5) of the NC is almost similar to that of PHPA (B-0.5) with or without pipe rotation but at the intermediate-sandstone size (2.00–2.40 mm) (Fig. 19), the NC showed higher CTEs than the PHPA. Similarly, for the largest cuttings size (2.80–3.20 mm) measured at the vertical annulus (0°) (Fig. 20), the NC showed the highest CTE than the base mud and PHPA by 24.3% and 4.1% (without pipe rotation) and by 17% and 2.3% (with pipe rotation), respectively. In turn, the PHPA improved the CTE of the BM by 14.2% and 19.4% with and without pipe rotation, respectively. The formation of electrostatic attractive force between the NC and water molecules help to increase the colloidal interaction of the mud with cuttings that led to the transportation of the cuttings to the surface (Medhi et al., 2020). The PHPA can be efficient at a low concentration owing to its ability to entangle. The long-chains of bonded monomers increases

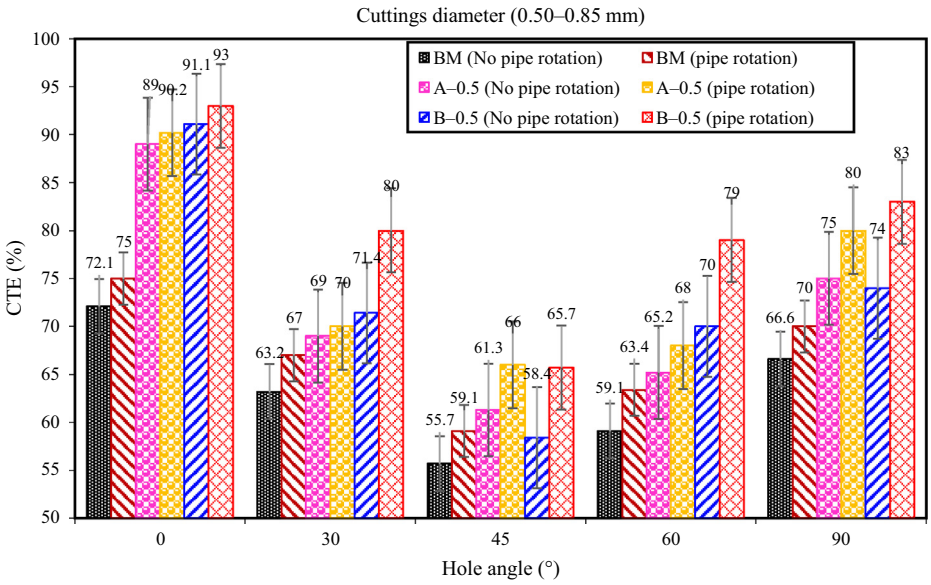

Fig. 17 CTE at different hole angles and mud systems for cuttings size of 0.50–0.85 mm (using a fixed flow rate of 42 L/min) with and without pipe rotation.

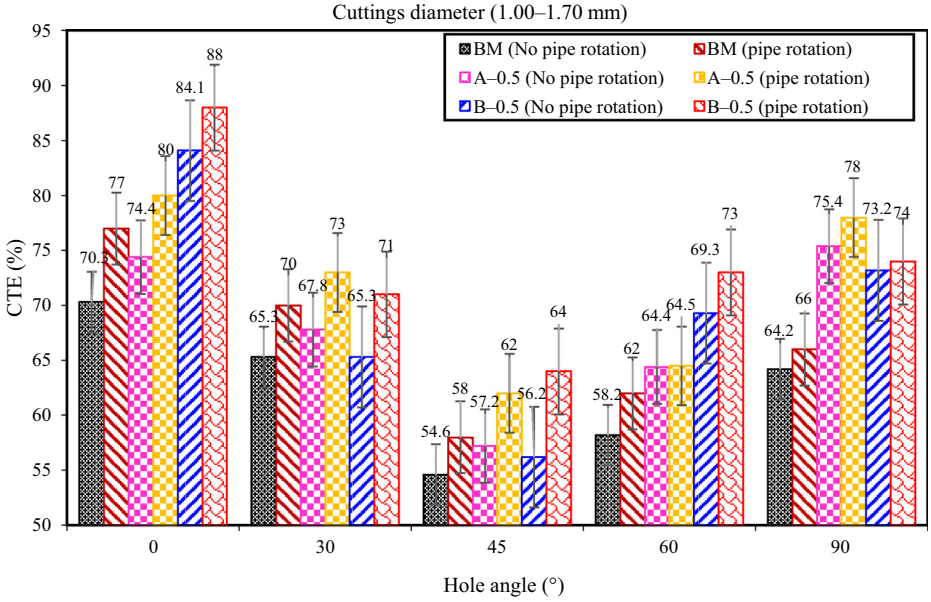

Fig. 18 CTE at different hole angles and mud systems for cuttings size of 1.00–1.70 mm (using a fixed flow rate of 42 L/min) with and without pipe rotation.

the viscosity of PHPA because the entanglement of these chains causes the structure to become larger, and thus, the increase in cuttings transport (Lam et al., 2015).

A further observation from these figures substantiates that the three mud systems applied have slightly better percent cuttings transported when the pipe was rotated than when it was in a static condition at all cuttings sizes and hole angles. With the smallest cuttings size (0.50–0.85 mm) at angle 60° (Fig. 17), the application of pipe rotation improved the CTE of the mud systems by 7.5% of the BM, 4.3% of NC, and 10% of PHPA. At this angle, the PHPA mud system lifted the highest cuttings to the surface. According to the reports of previous research by Ozbayoglu et al. (2008), pipe rotation has a moderate effect in carrying cuttings by the flowing mud stream, and the effect can be significant if the pipe is making an orbital motion. The orbital motion of the pipe can mechanically disturb cuttings accumulation and concentration, and expose the cuttings to where higher annular velocity exists for easier lifting to the annulus.

Different hole angles were also considered to determine the most critical in the lifting process of cuttings. Looking at all the plots shown in Figs. 17–20, it showed that the percent cuttings transported by the muds decreased with increasing cuttings diameters at all hole angles with or without pipe rotation. The highest cuttings recovered occurred in the verti-

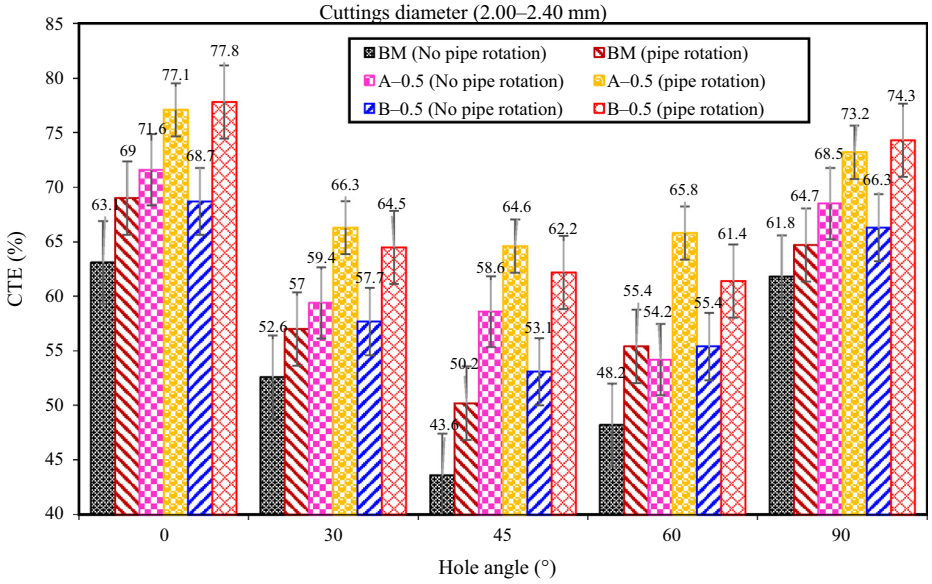

Fig. 19 CTE at different hole angles and mud systems for cuttings size of 2.00–2.40 mm (using a fixed flow rate of 42 L/min) with and without pipe rotation.

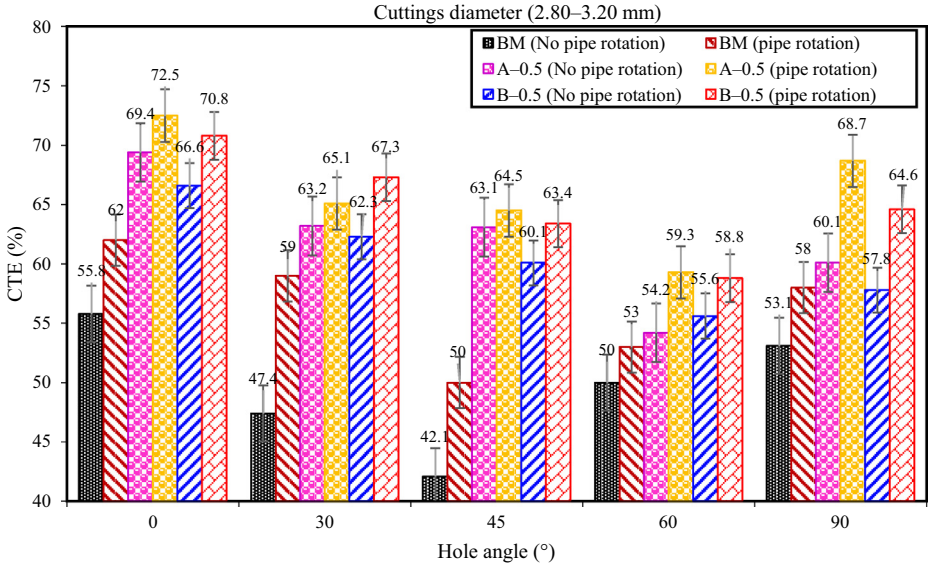

Fig. 20 CTE at different hole angles and mud systems for sandstone grains size of 2.80–3.20 mm (using a fixed flow rate of 42 L/min) with and without pipe rotation.

cal annulus (0°). This is because of the less complicated nature of the hole architecture that is governed by the gravity effect, the viscosity of the mud, and the pump flow rate. Once sufficient flow rate and viscosity are applied, the gravity effects on cuttings will be overcome and cuttings will transport out of the hole. This implies that cuttings move downward with no circulation and upward with circulation. Next, the percent cuttings recovered at horizontal annulus (90°) was the second-highest because the dominant force (axial drag force) responsible for the cuttings lifting from this pipe angle was not affected by hole inclination, and hence, the cuttings will not slip provided the mud circulation is in progress. The CTE at 30° inclinations was the third-highest, and such annulus is considered as low–inclination angles because cuttings settling is typically low (Ozbayoglu et al., 2008). With more observation on all the plots of Figs. 17–20, an improved CTE was seen at 60° hole-angle over that of the 45° inclination. This implies that the 45° hole-angle was the most difficult angle to clean in this study. At this angle, the CTE of the modified NC was better than that of the PHPA for intermediate-size cuttings of 2.00–2.40 mm by 3.7% and 9.4% with and without pipe rotation, respectively (Fig. 19). A similar phenomenon occurred at this angle with that of 2.80–3.20 mm cuttings size (Fig. 20), where the NC leads the PHPA in the cleaning process by 4.9% (without) and 3.7% (with) pipe rotation. The pipe angles (45° and 60°) experienced the least wellbore cleaning because of the higher tendency of cuttings to gravitate to the low side of the hole even with circulation at these angles. Also, at these angles

cuttings do not recycle readily and are difficult to re-enter the mud stream when they hit the bottom of the hole (Katende et al., 2019). According to the cuttings performance indicator (CTE), hole angle 45° needs special attention while drilling. Pipe rotation with high annular velocity could be more effective to clear cuttings from the drilled hole but caution should be taken in increasing flow rate to minimize frictional pressure losses.

5. Conclusions

In this study, the influence of different parameters, such as annular velocities from 66 to 138.6 ft/min, cuttings diameters between 0.50 and 3.20 mm, and a constant hole angle inclination of 60° on the cuttings transport performance of a modified NC drilling mud was investigated. A concentration of 0.5 ppb at a pump rate of 42 L/min (0.042 m^3/min) and different hole angle inclinations (0°, 30°, 45°, 60°, and 90°) were used to compare between the cuttings transport efficiency of modified NC and PHPA in the presence of 150 rpm. The ζ-potential data validate that PP-SiO_2 NC-NH_2 has strong stability and dispersibility in WBMs. PSD results authenticate the success of the modification process and corroborated that the modified NC particles have a narrow size distribution between 80 and 390 nm, which is within the range of nanometric-scale. The success of this modification process was supported by TEM investigation. Improvement in rheological properties was observed with the concentrations of modified NC performed at two different temperatures of 78 and 300 °F and it confirms beneficial effect for drilling mud applications and improvement in the efficiency of cuttings transport. Also, a significant increase in the rheological properties of the BM with PHPA was observed, which might not be suitable for effective hole cleaning. The CTE values of 0.5 ppb PHPA and those of the modified NC are comparable, but that of the modified NC exhibited higher CTE with larger cuttings sizes. The modified NC drilling muds showed higher CTEs than the BM with or without pipe rotation because of their increased colloidal interactions with cuttings. The vertical hole (0°) was the best in the hole cleaning process, followed by 90°, 30°, and 60° annuli. Hole inclination 45° was the worst angle in the wellbore cleaning process. The highest annular velocity, mud viscosity, and 150 rpm exhibited the greatest increasing impact on CTE. The inclusion of modified NC in conventional WBM displayed promising results in the cuttings transport process and is proposed for drilling operation provided it has good dispersibility.

CRediT authorship contribution statement

Jeffrey O. Oseh: Conceptualization, Data curation, Formal analysis, Investigation, Methodology, Visualization, Writing - original draft, Writing - review & editing. **M.N.A.M. Norddin:** Conceptualization, Data curation, Formal analysis, Project administration, Resources, Supervision, Validation, Writing - review & editing. **Issham Ismail:** Data curation, Project administration, Resources, Supervision, Validation. **Afeez O. Gbadamosi:** Software. **Augustine Agi:** Software. **Abdul R. Ismail:** Conceptualization, Project administration. **Prasad Manoger:** Formal analysis, Investigation, Methodology, Visualization. **Kumaresan Ravichandran:** Investigation, Methodology, Visualization.

Declaration of Competing Interest

The authors declare that they have no known competing financial interests or personal relationships that could have appeared to influence the work reported in this paper.

Acknowledgments

The authors wish to thank the Ministry of Higher Education Malaysia (MOHE) and Universiti Teknologi Malaysia Research Management Centre for funding this project under the Fundamental Research Grant Scheme (FRGS) with reference number FRGS/1/2019/TK05/UTM/02/20.

Appendix A. Supplementary material

Supplementary data to this article can be found online at https://doi.org/10.1016/j.arabjc.2020.07.004.

References

API recommended practice 13B-1, 2017. API standard practice for field testing water–based drilling fluids, fifth ed. pp. 1–121.

Barry, M.M., Jung, Y., Lee, J.K., 2015. Fluid filtration and rheological properties of nanoparticle additive and intercalated clay hybrid bentonite drilling fluids. J. Petrol. Sci. Eng. 127 (3), 338–346.

Bitinis, N., Hernandez, M., Verdejo, R., Kenny, J.M., Lopez-Manchado, M.A., 2011. Recent advances in clay/polymer nanocomposites. Adv. Mater. 23, 229–5236.

Boyou, N.V., Ismail, I., Sulaiman, W.R.W., Haddad, A.S., Hussein, N., Heah, T.H., Nadaraja, K., 2019. Experimental investigation of hole cleaning in directional drilling by using nano-enhanced water-based drilling fluids. J. Pet. Sci. Eng. 176, 220–231. https://doi.org/10.1016/j.petrol.2019.01.063.

Caenn, R., Darley, H.C.H., Gray, G.R., 2017. Introduction to drilling fluids. In: Composition and properties of drilling and completion fluids, 7th ed. Gulf Professional Publishing, USA, pp 1–748. ISBN: 978-0-12-804751-4.

Cao, J., Song, T., Zhu, Y., Wang, S., Wang, X., Lv, F., Sun, M., 2017. Application of amino-functionalized nanosilica in improving the thermal stability of acrylamide-based polymer for enhanced oil recovery. Energy Fuels 32 (1), 246–254. https://doi.org/10.1021/acs.energyfuels.7b03053.

Elochukwu, H., Gholami, R., Dol, S.S., 2017. An approach to improve the cuttings carrying capacity of nanosilica based muds. J. Pet. Sci. Eng. 152, 309–316. https://doi.org/10.1016/j.petrol.2017.03.008.

Fattah, K.A., Lashin, A., 2016. Investigation of mud density and weighting materials effect on drilling fluid filter cake properties and formation damage. J. Afr. Earth Sc. 117, 345–357. https://doi.org/10.1016/j.jafrearsci.2016.02.003.

Gbadamosi, A.O., Junin, R., Abdalla, Y., Agi, A., Oseh, J.O., 2018a. Experimental investigation of the effects of silica nanoparticle on hole cleaning efficiency of waterbased drilling mud. J. Pet. Sci. Eng. 172, 1226–1230. https://doi.org/10.1016/j.petrol.2018.09.097.

Gbadamosi, A.O., Junin, R., Manan, M.A., Augustine, A., Oseh, J.O., Usman, J., 2019. Synergistic application of aluminum oxide nanoparticles and oilfield polyacrylamide for enhanced oil recovery. J. Pet. Sci. Eng. https://doi.org/10.1016/j.petrol.2019.106345.

Gbadamosi, A.O., Junin, R., Oseh, J.O., Agi, A., Yekeen, N., Abdalla, Y., Ogiriki, S.O., Yusuff, A. S., 2018b. Improving hole cleaning efficiency using nanosilica in water-based drilling mud. SPE Nigeria Annual International Conference and Exhibition. doi: 10.2118/193401-ms.

Hale, A.H., Mody, F.K., 1993. Partially hydrolyzed polyacrylamide (PHPA) mud systems for Gulf of Mexico deep-water prospects. In:

SPE International Symposium on Oilfield Chemistry, 2–5 March, New Orleans, Louisiana. pp. 301–316. https://doi.org/10.2118/25180-MS.

Ismail, I., Onuoha, M.D.U., Ismail, A.R., Piroozian, A., Sulaimon, W. R.W., Abbda, S.M., 2016. Improving drilled cuttings lifting using polypropylene beads in water-based mud at different annular mud velocities. Int. J. Eng. Technol. 9, 1–10.

ISO 13320-1, 2009. Particle size analysis. Laser diffraction methods. Part 1: General principles.

Jafarzadeh, M., Ab, A.I., Sipaut, C.S., 2012. Synthesis of silica–polypyrrole core–shell nanocomposite using in situ γ-aminopropyltriethoxysilane (APTES)-modified nanosilica. Synthetic Metals 162 (5–6), 466–476.

Jain, R., Mahto, V., Sharma, V.P., 2016. Evaluation of polyacrylamide grafted polyethylene glycol/silica nanocomposite as potential additive in water based drilling mud for reactive shale formation. J. Nat. Gas Sci. Eng. 26, 526–537.

Katende, A., Segar, B., Ismail, I., Sagala, F., Saadiah, H.H.A.R., Samsuri, A., 2019. The efect of drill–pipe rotation on improving hole cleaning using polypropylene beads in water based mud at diferent hole angles. J. Pet. Explor. Prod. Technol., 1–10 https://doi.org/10.1007/s13202-019-00815-1.

Lam, C., Martin, P.J., Jefferis, S.A., 2015. Rheological properties of PHPA polymer support fluids. J. Mater. Civ. Eng. 27 (04015021). https://doi.org/10.1061/(asce)mt.1943-5533.0001252.

Luz, R.C.S., Fagundes, F.P., Balaban, R.C., 2017. Water-based drilling fluids: the contribution of xanthan gum and carboxyl methyl cellulose on filtration control. Soc. Petrol. Eng. J. 71, 365–2373. https://doi.org/10.1007/s11696-017-0231-.

Lyons, W.C., Carter, T., Lapeyrouse, N.J., 2016. All the formulas you need to solve drilling and production problems. In: 4 ed(s); Formulas and Calculations for Drilling, Production, and Workover, USA, Gulf Professional Publishing. pp. 357–381.

Mao, H., Qiu, Z., Shen, Z., Huang, W., 2015. Hydrophobic associated polymer based silica nanoparticles composite with core–shell structure as a filtrate reducer for drilling fluid at ultra-high temperature. J. Pet. Sci. Eng. 129, 1–14. https://doi.org/10.1016/j.petrol.2015.03.003.

Medhi, S., Chowdhury, S., Gupta, D.K., Mazumdar, A., 2020. An investigation on the effects of silica and copper oxide nanoparticles on rheological and fluid loss property of drilling fluids. J. Pet. Expl. Prod. Tech. 10, 91–100.

Omurlu, C., Pham, H., Nguyen, Q.P., 2016. Interaction of surface-modified silica nanoparticles with clay minerals. Appl. Nanosci. 6 (8), 1167–1173. https://doi.org/10.1007/s13204-016-0534-y.

Oseh, J.O., Mohd Norddin, M.N.A., Ismail, I., Gbadamosi, A.O., Agi, A., Ogiriki, S.O., Ismail, A.R., 2019b. Performance evaluation of a benign oil - based mud from non - edible sweet almond seed prunus amygdalus dulcis oil. In: Paper SPE 198717-MS Presented at the SPE Nigeria Annual International Conference and Exhibition, 5-7 August, Lagos, Nigeria. https://doi.org/10.2118/198717-MS.

Oseh, J.O., Mohd, M.N.A., Farooqi, F., Ismail, A.R., Ismail, I., Gbadamosi, A.O., Agi, A., 2019c. Experimental investigation of the effect of henna leaf extracts on cuttings transportation in highly deviated and horizontal wells. J. Petrol. Explor. Prod. Technol. 9, 2387–2404. https://doi.org/10.1007/s13202-019-0631-z.

Oseh, J.O., Mohd Norddin, M.N.A., Ismail, I., Ismail, A.R., Gbadamosi, A.O., Agi, A., Ogiriki, S.O., 2019a. Investigating almond seed oil as potential biodiesel based drilling mud. J. Pet. Sci. Eng. 181 (106201), 1–15. https://doi.org/10.1016/j.petrol.2019.106201.

Oseh, J.O., Mohd Norddin, M.N.A., Ismail, I., Gbadamosi, A.O., Agi, A., Ismail, A.R., 2020a. Study of cuttings lifting with different annular velocities using partially hydrolyzed polyacrylamide and enriched polypropylene–nanosilica composite in deviated and horizontal wells. Applied Nanoscience 10 (3), 971–993.

Oseh, J.O., Mohd Norddin, M.N.A., Muhamad, H.N., Ismail, I., Gbadamosi, A.O., Agi, A., Ismail, A.R., Blkoor, S.O., 2020b. Influence of (3–Aminopropyl) triethoxysilane on entrapped polypropylene at nanosilica composite for shale swelling and hydration inhibition. Journal of Petroleum Science and Engineering 194 (107560), 1–16.

Ozbayoglu, E.M., Saasen, A., Sorgun, M., Svanes, K., 2008. Effect of pipe rotation on hole cleaning for water-based drilling fluids in horizontal and deviated wells. In: IADC/SPE Asia Pacific Drilling Technology Conference and Exhibition, pp. 1–11. https://doi.org/10.2118/114965-ms.

Qiao, B., Wang, T.J., Ga, H., Jin, Y., 2015. High density silanization of nano-silica particles using γ-aminopropyltriethoxysilane (APTES). Appl. Surf. Sci. 351, 646–654. https://doi.org/10.1016/j.apsusc.2015.05.174.

Song, K.W., Kim, Y.S., Chan, G.S., 2006. Rheology of concentrated xanthan gum solutions: steady shear flow behavior. Fibers Polym. 7 (2), 129–138.

Thangaraj, B., Jia, Z., Dai, L., Liu, D., Du, W., 2019. Effect of silica coating on Fe3O4 magnetic nanoparticles for lipase immobilization and their application for biodiesel production. Arabian J. Chem. 12 (8), 4694–4706. https://doi.org/10.1016/j.arabjc.2016.09.004.

Wang, Y., Li, Y., Zhang, R., Huang, L., He, W., 2006. Synthesis and characterization of nanosilica/polyacrylate composite latex. Polym. Compos. 27 (3), 282–288.

Wiśniowski, R., Skrzypaszek, K., Małachowski, T., 2020. Selection of a suitable rheological model for drilling fluid using applied numerical methods. Energies 13 (12), 3192. https://doi.org/10.3390/en13123192.

Xu, J., Qiu, Z., Zhao, X., Zhong, H., Li, G., Huang, W., 2018. Synthesis and characterization of shale stabilizer based on polyethylene glycol grafted nano-silica composite in water-based drilling fluids. J. Pet. Sci. Eng. 63, 371–377. https://doi.org/10.1016/j.petrol.2018.01.007.

Youssef, A.M., Malhat, F.M., Abdel Hakim, A.A., Dekany, I., 2017. Synthesis and utilization of poly (methylmethacrylate) nanocomposites based on modified montmorillonite. Arabian J. Chem. 10 (5), 631–642. https://doi.org/10.1016/j.arabjc.2015.02.017.

Zu, L., Li, R., Jin, L., Lian, H., Liu, Y., Cui, X., 2013. Preparation and characterization of polypropylene/silica composite particle with interpenetrating network via hot emulsion sol-gel approach. Progr. Nat. Sci.: Mater. Int. 24, 42–49.